Eur. Phys. J. A **3**, 361–371 (1998)

THE EUROPEAN PHYSICAL JOURNAL A

Study of the $\pi^0\pi^0$-system with the GAMS-4000 spectrometer at 100 GeV/c

GAMS Collaboration: IHEP[1]–IISN[2]–LANL[3]–LAPP[4]–KEK[5] (Joint CERN–IHEP experiment)

D. Alde[3], F.G. Binon[7], M. Boutemeur[6], C. Bricman[2], S.V. Donskov[1], M. Gouanère[4], A.V. Inyakin[1], S. Inaba[5], V.A. Kachanov[1], G.V. Khaustov[1], E.A. Knapp[3], A.A. Kondashov[1], A.A. Lednev[1], V.A. Lishin[1], J.P. Peigneux[4], M. Poulet[4], Yu.D. Prokoshkin[1,a], S.A. Sadovsky[1], V.D. Samoylenko[1], P.M. Shagin[1], A.V. Singovsky[4], J.P. Stroot[2], V.P. Sugonyaev[1], K. Takamatsu[8], T. Tsuru[5]

[1] Institute for High Energy Physics, Protvino 142284, Russia
[2] Institut Interuniversitaire des Sciences Nucléaires, B-1050 Brussels, Belgium
[3] Los Alamos National Laboratory, Los Alamos, NM 87544, USA
[4] Laboratoire d'Annecy de Physique des Particules, F-74019 Annecy-le-Vieux, France
[5] National Laboratory for High Energy Physics — KEK, Tsukuba, Ibaraki 305, Japan
[6] CERN, CH-1211 Geneva 23, Switzerland
[7] Université Libre de Bruxelles, CP 229, B-1050 Brussels, Belgium
[8] Miyazaki University, Miyazaki 889-21, Japan

Received: 26 July 1998
Communicated by V.V. Anisovich

Abstract. The $\pi^0\pi^0$-system produced in the charge exchange $\pi^- p$-reaction at 100 GeV/c has been studied. The experiment was performed at the CERN SPS accelerator with the multiphoton hodoscope spectrometer GAMS-4000. A partial wave analysis was carried out in the mass range from 0.8 GeV to 3.0 GeV at $-t < 0.2$ (GeV/c)^2 with the S, D, G and J waves. The S-wave exhibits rather complicated behaviour with a series of four bumps separated by three dips, at 1 GeV, 1.5 GeV and 2 GeV, which give the evidence for several scalar resonances. Clear peaks corresponding to the $f_2(1270)$, $f_4(2050)$ and $f_6(2510)$ mesons are seen in the higher waves. All the three mesons are produced via a dominating one pion t-channel exchange. The parameters and production cross sections of these mesons are measured.

PACS. 14.40.Cs Other mesons with S = C = 0, mass <2.5 GeV

1 Introduction

In this paper the GAMS Collaboration presents a study of the $\pi^0\pi^0$-system produced in the charge exchange reaction

$$\begin{array}{l} \pi^- p \to M^0 n \\ \qquad\quad \big\lfloor\!\!\to \pi^0\pi^0 \to 4\gamma \end{array} \qquad (1)$$

at 100 GeV/c π^- beam momentum.

In the previous analyses of this reaction performed by the GAMS Collaboration at 38 GeV/c [1–5], a series of interesting results was obtained. A complicated bump-dip structure of the S-wave at low momentum transfer was revealed. A simultaneous analysis of the GAMS data on the S-waves in the $\pi^0\pi^0$, $\eta\eta$ and $\eta\eta'$ systems together with the data of other experiments [6] indicated the existence of five resonances with quantum numbers $I^G J^{PC} = 0^+0^{++}$ in the mass range below 1.9 GeV while the quark model predicts only four. One of the five resonances is superfluous for the $q\bar{q}$-classification. This state is considered as a ground state scalar glueball candidate. The production mechanisms of the $f_0(980)$, $f_2(1270)$ and $f_4(2050)$ were studied at different momentum transfer, a strong upper limit on the production cross section of the $f_2(1810)$ in the $\pi^0\pi^0$-system was set.

The investigation of the $\pi^0\pi^0$-system at 100 GeV/c provides a way to get on to the high mass region where a spin 6 resonance $f_6(2510)$ was previously observed by the GAMS Collaboration [7]. Study of the high mass region is also important for another reason. Recently an interest to the scalar isoscalar mesons has increased in connection with a search for a scalar glueball. The data on the S-wave $\pi\pi$-amplitude are very important for the classification of the 0^+0^{++} mesons and for the identification of states with an enhanced gluonic component. Meanwhile the information on the S-wave above 1.7–1.8 GeV is now rather scanty and contradictory. The S-wave separation at

[a] Deceased

high masses is impossible without a detailed partial wave analysis (PWA) because the contribution of this wave is hidden by the higher spin waves which dominate in reaction (1) at mass above 1 GeV.

In the present work a PWA is performed in a wide mass range from 0.8 GeV to 3 GeV at values of four momentum transfer squared $-t < 0.2$ (GeV/c)^2.

2 Event selection

The experimental data were collected at the CERN SPS accelerator during two runs of measurements in 1984. The multiphoton spectrometer GAMS-4000 was used to detect γ-quanta in the reaction (1) final state. The spectrometer comprised a matrix of 64×64 lead glass cells of transverse size 38×38 mm^2. A hole of 2×2 cells was made in the center for the beam particles not interacting with the liquid hydrogen target to pass. The distance between the target and the γ-spectrometer was equal to 15 m. This allowed one to efficiently detect photons from π^0 decays in the $\pi^0\pi^0$ mass range up to 3 GeV. The experimental setup, the data acquisition system, the GAMS-4000 calibration procedures were described in detail [8,9].

Multiplicity of photons, their energies and impact point coordinates in GAMS for each event are determined using a geometrical reconstruction program [10]. Only 4γ events are retained to separate the $\pi^0\pi^0$-system. A series of cuts is applied to reduce the instrumental background and decrease event leakage from a class with photon multiplicity k to classes with multiplicities $k-1$ or $k+1$. The γ-quanta pair is treated as one γ-quantum if the invariant mass of the pair is less than 25 MeV and the distance between γ-quanta is less than 35 mm. The energy of each photon is required to be larger than the threshold which increases exponentially from 0.6 GeV at GAMS edges to 2.5 GeV in the center. This cut allows one to reject the false photons generated by the sensitive reconstruction program due to fluctuations of the energy deposited in γ-spectrometer cells and to electronic noises. The minimum distance between beam axis and photon impact point in GAMS is required to be larger than 60 mm in order to suppress the background associated with a heavy load of the central cells. This cut decreases also the distortions due to the electromagnetic shower leakage into the central hole. The total energy release in GAMS is confined within the 10% range of the beam energy.

The quality of the selected 4γ events is demonstrated in Fig. 1, where the invariant mass of γ-pair is shown when the second pair is identified as π^0 (100 MeV$< m_{2\gamma} <$ 170 MeV). It is clearly seen from the figure that the background under π^0 peak does not exceed 1%.

The final separation of the $\pi^0\pi^0$-system from other possible 4γ-channels ($\pi^0\eta$, $\eta\eta$, $\pi^0\eta'$ and $\eta\eta'$) is carried out on the basis of kinematical analysis (3C fit, masses of recoil neutron and two mesons being fixed). The events are selected with the best χ^2 for the $\pi^0\pi^0$ hypothesis ($\chi^2 < 8.3$, 97% confidence level). A total of 644,000 $\pi^0\pi^0$ events is selected. Only events with $-t < 0.2$ (GeV/c)^2 where one pion exchange (OPE) dominates (see, for example, [1]) are retained for further consideration. Outside this range 21% of all $\pi^0\pi^0$ events lies.

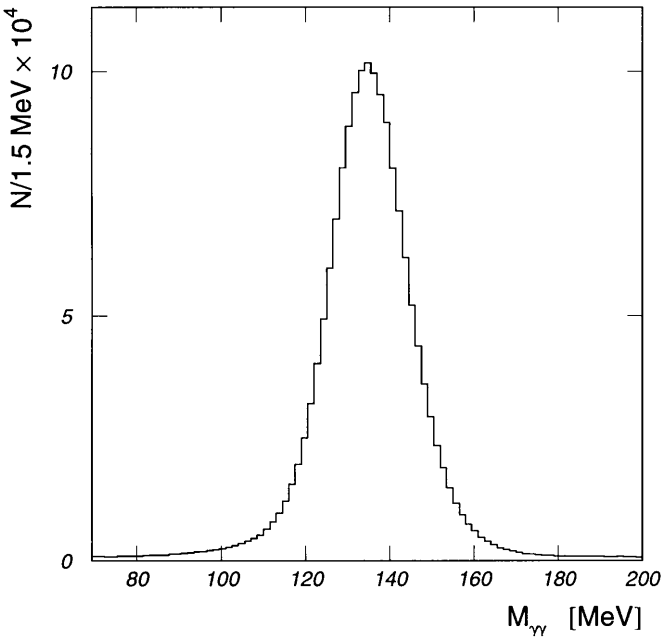

Fig. 1. Invariant mass of γ-pair when the second pair is identified as π^0

3 Mass spectrum

Mass spectrum of the $\pi^0\pi^0$-system obtained after kinematical analysis at $-t < 0.2$ (GeV/c)^2 is presented in Fig. 2. It demonstrates the same characteristic features as that at 38 GeV/c. It is dominated by the $f_2(1270)$, a dip at 1 GeV is seen which corresponds to the $f_0(980)$. Above the $f_2(1270)$, a peak is clearly seen with a mass of about 2 GeV, it is interpreted with the $f_4(2050)$. A peak at 1.7 GeV cannot be identified with any known resonance. It may be connected with the S-wave contribution. The PWA is necessary to get an exact answer. A small shoulder is seen above the $f_4(2050)$ peak at 2.4 GeV, where the $f_6(2510)$ was observed previously by the GAMS Collaboration [7].

In the OPE approximation, the reaction (1) angular distribution can be written in the form

$$I(\cos\theta_{\rm GJ}) \sim \left|\sum_l A_l P_l(\cos\theta_{\rm GJ})\right|^2, \qquad (2)$$

where A_l is the spin l amplitude, $P_l(x)$ is the Legendre polynomial, $\theta_{\rm GJ}$ is the Gottfried-Jackson angle. The angular distributions for the high spin mesons are characterized by a series of minima and maxima, as follows from (2). This allows one to enhance or suppress a signal from the considered resonance by choosing a suitable $\cos\theta_{\rm GJ}$-interval. In the interval $0.75 < \cos\theta_{\rm GJ} < 0.85$ a function $[P_6(\cos\theta_{\rm GJ})]^2$ reaches its maximum while a polynomial $P_4(\cos\theta_{\rm GJ})$ squared is close to zero. In the mass spectrum

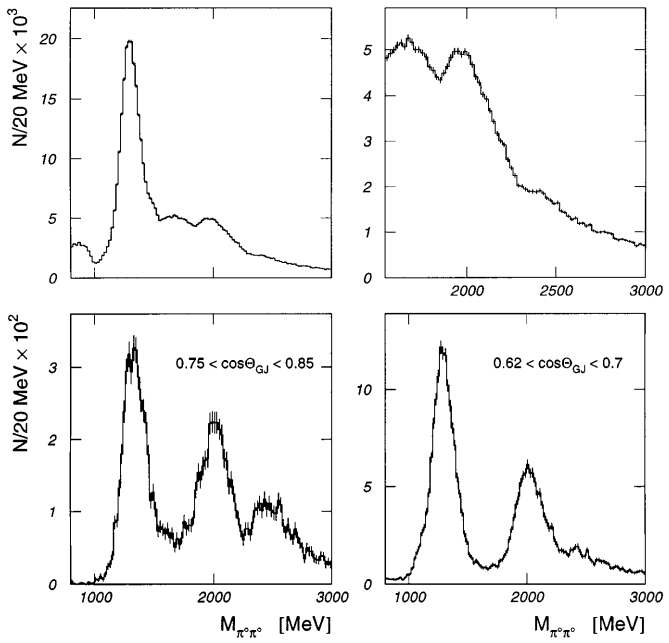

Fig. 2. Two upper plots show mass spectrum of the $\pi^0\pi^0$-system after kinematical 3C fit, $|t| < 0.2$ (GeV/c)^2 (high mass region is shown in the right plot). Two lower plots show $\pi^0\pi^0$ mass spectra in the $\cos\theta_{\rm GJ}$-intervals where spin 6 contribution is enhanced (left plot) or supressed (right plot)

built for the events from this interval, a clear $f_6(2510)$ peak is seen along with the $f_2(1270)$ and $f_4(2050)$. To the contrary, for the events from the $0.62 < \cos\theta_{\rm GJ} < 0.7$ interval where a polynomial $[P_6(\cos\theta_{\rm GJ})]^2$ has a minimum, an $f_4(2050)$ peak is clearly seen, while a signal from the $f_6(2510)$ is absent (Fig. 2).

Further study of the structures observed in the mass spectrum is performed on the basis of PWA.

4 Partial wave analysis

4.1 Detection efficiency

Detection efficiency for the reaction (1) events ε is computed by the Monte Carlo method as a function of four significant dynamical variables: $M_{\pi\pi}$, t and two angles in the Gottfried-Jackson frame, $\theta_{\rm GJ}$ and $\phi_{\rm TY}$. The event kinematics is simulated up to the final decay of each π^0 to two photons taking into account beam characteristics (dispersions in the energy and the transversal size) and all the geometrical parameters of the setup. A profile of real showers is used to simulate the electromagnetic showers in GAMS [10], fluctuations of energy released in the spectrometer cells covered by the showers are included. The MC events are then processed with the very same programs as in the case of the experimental data. This procedure takes into account in detail the setup parameters, the measurement conditions and all stages of the event selection used in the physical data analysis.

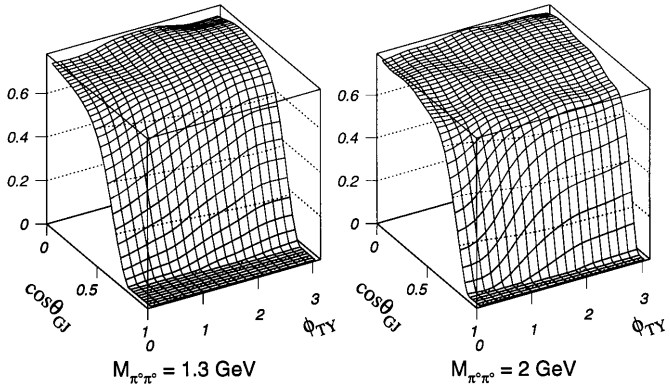

Fig. 3. Detection efficiency of the reaction (1) events integrated over t from 0 to 0.2 (GeV/c)^2 at $M_{\pi\pi} = 1.3$ GeV and 2 GeV

The MC events are generated uniformly distributed over variables $\cos\theta_{\rm GJ}$, $\phi_{\rm TY}$ and $e^{\alpha t}$, $\alpha = 5$ (GeV/c)$^{-2}$, in the mass points equally spaced with 100 MeV step in an interval from 0.6 GeV to 3 GeV. A total of 15 million MC events are generated.

The efficiency is parametrized by the method of [11] and represented in the form of 4-dimensional Fourier series:

$$\varepsilon(\theta_{\rm GJ},\phi_{\rm TY},t,M_{\pi\pi}) = \sum_{lmkn} \varepsilon_{lmkn} {\rm Re}\,\{Y_l^m(\theta_{\rm GJ},\phi_{\rm TY})\}\,P_k(a_1+b_1e^{\alpha t}) \times P_n(a_2+b_2M_{\pi\pi}), \quad (3)$$

where $Y_l^m(\theta_{\rm GJ},\phi_{\rm TY})$ is the spherical harmonic, $P_k(x)$ is the Legendre polynomial.

Two-dimensional efficiency calculated in two mass points, 1.3 GeV and 2 GeV, integrated over t in interval $0-0.2$ (GeV/c)^2 is presented in Fig. 3. The efficiency achieves a maximum at $\cos\theta_{\rm GJ} \approx 0$ and reduces to zero at $\cos\theta_{\rm GJ} \to 1$. A zone of zero efficiency increases rapidly with the decrease in mass, it occupies about 22% of phase volume in the $f_2(1270)$ region. At high masses ε is equal to zero only in a small part of phase space near $\cos\theta_{\rm GJ} \approx 1$. The efficiency integrated over $\cos\theta_{\rm GJ}$, $\phi_{\rm TY}$ and t reaches a maximum at $M_{\pi\pi} \approx 2.2$ MeV and then decreases only slightly with the increase in mass up to 3 GeV. This provides favorable conditions for PWA at high masses.

4.2 Angular distributions

The angular distribution of the reaction (1) events in the Gottfried-Jackson frame is given by a sum of two non-interfering terms

$$I(\theta_{\rm GJ},\phi_{\rm TY}) = |h_0(\theta_{\rm GJ}) + h_-(\theta_{\rm GJ})\cos\phi_{\rm TY}|^2 + |h_+(\theta_{\rm GJ})\sin\phi_{\rm TY}|^2. \quad (4)$$

The first term in Eq. (4) corresponds to the exchange with unnatural-parity in the reaction (1) t-channel, the second one describes the natural-parity exchange. Only

the waves with spin $l \leq l_m = 6$ are taken into account in the PWA. The higher spin contribution is negligible in the mass range under study. The function h_0 includes the amplitudes with spin z-projections $m = 0$, the amplitudes with $|m| = 1$ form the functions h_- and h_+. The waves with $|m| > 1$ are negligibly small in the whole mass range. The functions h_0, h_- and h_+ can be written in terms of amplitudes of the S, D, G and J waves, corresponding to spin values 0, 2, 4 and 6, as follows

$$\begin{aligned}\sqrt{4\pi}h_0(\theta_{\rm GJ}) &= SP_0^0(\cos\theta_{\rm GJ}) + \sqrt{5}D_0P_2^0(\cos\theta_{\rm GJ}) \\ &+ \sqrt{9}G_0P_4^0(\cos\theta_{\rm GJ}) \\ &+ \sqrt{13}J_0P_6^0(\cos\theta_{\rm GJ}), \qquad (5)\\ \sqrt{4\pi}h_\pm(\theta_{\rm GJ}) &= \sqrt{3/5}D_\pm P_2^1(\cos\theta_{\rm GJ}) \\ &+ \sqrt{9/10}G_\pm P_4^1(\cos\theta_{\rm GJ}) \\ &+ \sqrt{13/21}J_\pm P_6^1(\cos\theta_{\rm GJ}), \qquad (6)\end{aligned}$$

where $P_l^m(\cos\theta_{\rm GJ})$ is the associated Legendre function.

Angular distribution (4) can be expanded in the spherical harmonic $Y_L^M(\Omega)$ series as follows

$$I(\Omega_{\rm GJ}) = \sum_{L=0}^{2l_m}\Big[t_L^0Y_L^0(\Omega_{\rm GJ}) + 2\sum_{M=1}^{2} t_L^M{\rm Re}\left\{Y_L^M(\Omega_{\rm GJ})\right\}\Big], \qquad (7)$$

where $\Omega_{\rm GJ} \equiv [\cos\theta_{\rm GJ}, \phi_{\rm TY}]$.

The PWA is carried out in 20 MeV mass bins (bin size is doubled at $M_{\pi\pi} > 1.5$ GeV). Events with $\varepsilon < 0.02$ are excluded from consideration. The experimental angular distributions are fitted independently in each mass bin $\Delta M_{\pi\pi}$ with the event-by-event maximum likelihood method. The MINUIT program [12] is used to minimize functional

$$F = -\sum_{i=1}^{N}\ln I(\Omega_i) + \sum_{LM} t_L^M\varepsilon_L^M, \qquad (8)$$

where N is the number of experimental events in $\Delta M_{\pi\pi}$ bin, ε_L^M are expansion (3) coefficients, calculated in the center of $\Delta M_{\pi\pi}$ bin and integrated over t taking into account the experimental t-distribution, t_L^M are spherical harmonic moments (7), expressed in terms of the partial amplitudes [13].

In the case of the S, D, G and J waves, angular distribution (4) is expressed via ten complex amplitudes (three amplitudes for each l, except for the S-wave which comes with only one amplitude). One amplitude, each for natural and unnatural spin-parities, can be set real, therefore, the angular distribution in each mass bin is characterized by 18 real parameters. Amplitude modules and relative phases of the partial waves are taken as parameters to be determined in PWA.

4.3 PWA ambiguity

A system of equations which expresses the t_L^M moments via the partial amplitudes [13] is bilinear and has, therefore, multiple solutions. Fit to the angular distributions gives only one solution in each mass bin, i.e. one set of parameters (amplitude modules and relative phases). All other solutions for the system of two pseudoscalar particles can be found with the well-known method [14,15]. First, the ambiguity problem is investigated for the partial waves with unnatural-parity exchange. For this purpose, continuous and continuously differentiated function is defined

$$\begin{aligned}g(\theta_{\rm GJ}) &= h_0(\theta_{\rm GJ}) + h_-(\theta_{\rm GJ}),\\ g(-\theta_{\rm GJ}) &= h_0(\theta_{\rm GJ}) - h_-(\theta_{\rm GJ}).\end{aligned} \qquad (9)$$

Introducing a variable $t = \tan(\theta_{\rm GJ}/2)$ and then $u = 1/t - t$ one can define a new function

$$G(u) = t^{-l_m}(1+t^2)^{l_m}g(t) = a_{l_m}\prod_{k=1}^{l_m}(u-u_k), \qquad (10)$$

which is a polynomial of order l_m and therefore can be expressed through its complex roots u_k (a_{l_m} is a complex constant).

One can replace any of the u_k roots by complex-conjugated one and calculate corresponding set of angular distribution parameters. These parameters are an equally valid solution because the reaction (1) angular distribution does not change under complex conjugation of the $G(u)$ roots (see [16]). Hence, there are, in general, 2^{l_m-1} non-trivial solutions for the waves with unnatural-parity exchange, after eliminating those which may be obtained by complex conjugation of the entire $G(u)$ function.

There are, therefore, 8 non-trivial solutions for unnatural-parity amplitudes in case of the S, D_0, $D_\pm$, G_0 and $G_\pm$ waves. The number of solutions increases to 32 if the J_0, J_- and J_+ waves are added.

When the ambiguity problem is resolved for the unnatural-parity amplitudes, natural-parity amplitudes can be found using the moments with $M = 2$, which can be expressed through the amplitudes with $|m| = 1$. An extra ambiguity for the waves with natural-parity exchange appears, if $l_m \geq 6$. This ambiguity may be eliminated by using the Ochs-Wagner model [17], which predicts the equality of the amplitudes with $|m| = 1$ for each l.

4.4 Bootstrapping procedure

The procedure described above allows one to solve the ambiguity problem in each mass bin. To link solutions in the adjacent mass bins, the requirements are introduced that real and imaginary parts of the $G(u)$ roots u_k be continuous and continuously differentiated functions of $M_{\pi\pi}$. For this purpose, the following functional is used

$$\Phi = \sum_{k=1}^{l_m}\frac{\left(a_k^{n-1} - a_{\lambda_k}^n\right)^2}{\left(\Delta a_k^{n-1}\right)^2 + \left(\Delta a_{\lambda_k}^n\right)^2} + \sum_{k=1}^{l_m}\frac{\left(a_k^{n-2} - 2a_k^{n-1} + a_{\lambda_k}^n\right)^2}{\left(\Delta a_k^{n-2}\right)^2 + 4\left(\Delta a_k^{n-1}\right)^2 + \left(\Delta a_{\lambda_k}^n\right)^2}, \qquad (11)$$

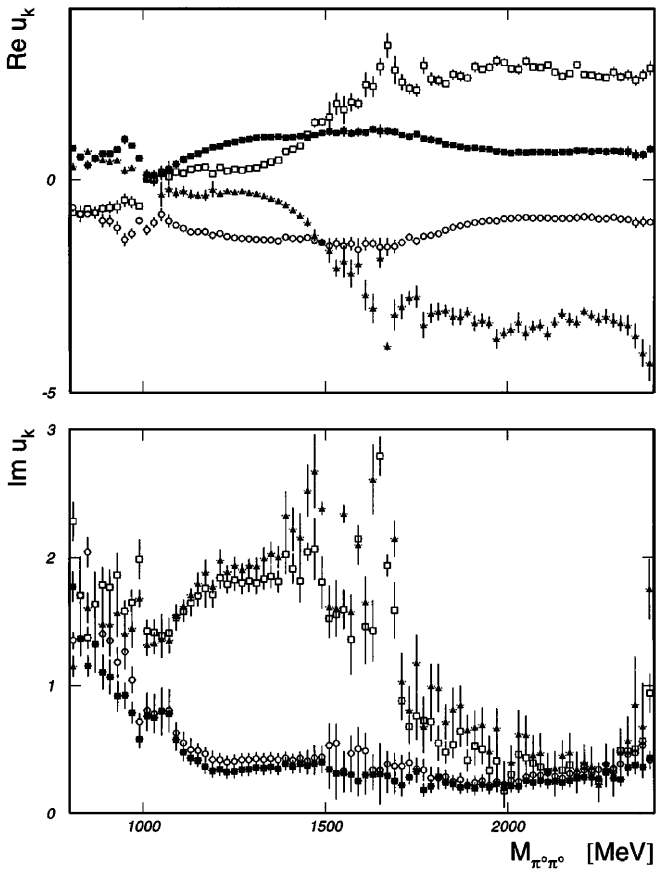

Fig. 4. Real and imaginary parts of $F(u)$ roots (see the text) as functions of mass obtained in PWA with S, D and G waves

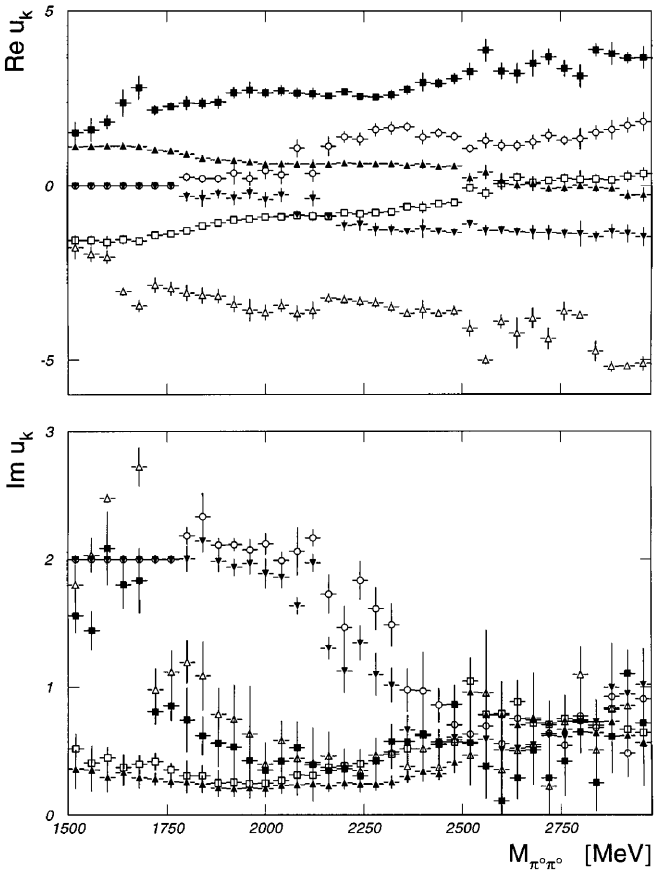

Fig. 5. The same as in Fig. 4 for the case of the S, D, G and J waves

where

$$a_k^n = \begin{cases} \mathrm{Re}\, u_k^n & \text{if } 1 \le k \le l_m, \\ |\mathrm{Im}\, u_k^n| & \text{if } l_m + 1 \le k \le 2l_m, \end{cases}$$

superscripts indicate the ordinal number of mass bin. Weight of each term in (11) depends on statistical errors of the real and imaginary parts of the roots entering this term.

All possible permutations of the roots $\{\lambda_k\}$ (in all $l_m!$) are sorted in n-th bin and the Φ value is calculated for each permutation (only the first term in (11) is taken into account for the first two bins). Finally, the roots in n-th bin are ordered in such a way that functional Φ has a minimal value.

The statistical errors of the roots in (11) are estimated by the Monte Carlo method. A total of 10 000 sets of the angular distribution parameters (amplitude modules and relative phases) are generated in each mass bin according to the Gaussian distributions with the mean values and the dispersions determined by MINUIT for one of the solutions. Then, roots of the $F(u)$ are calculated for each set, their real and imaginary parts are put in histograms. Dispersions of the obtained distributions are used as estimates of the statistical errors $\Delta\mathrm{Re}\, u_k^n$ and $\Delta\mathrm{Im}\, u_k^n$.

Figures 4 and 5 show the real and imaginary parts of the $F(u)$ roots as functions of mass (for the cases $l_m = 4$ and $l_m = 6$) after imposing the bootstrapping procedure. A behaviour of each root is clearly traced, the imaginary parts are well separated in those points where the real parts cross each other and vice versa, if the imaginary parts of two roots are close to each other, their real parts are separated quite well. It shows that the bootstrapping procedure based on functional (11) allows one to identify unambiguously all the PWA solutions in the whole mass range from 0.8 GeV to 3 GeV.

5 Partial wave analysis results

5.1 PWA in the mass region below 2.4 GeV

At the first stage, a PWA is carried out in the mass range from 0.8 GeV to 2.4 GeV taking into account S, D_0, D_-, D_+, G_0, G_- and G_+ waves. The detection efficiency drops sharply at low masses (in the $f_2(1270)$ region and below, see above) which makes difficult the PWA here. Because of this, some extra conditions are imposed at low masses. Modules of the G_0, G_- and G_+ amplitudes squared below 1.5 GeV are described by the exponential curves dropping fast and smoothly with decrease in mass and fixed. Similar constraints are applied to the D_0, D_- and D_+ waves below 1 GeV. The Ochs-Wagner model [17] predicts an equality

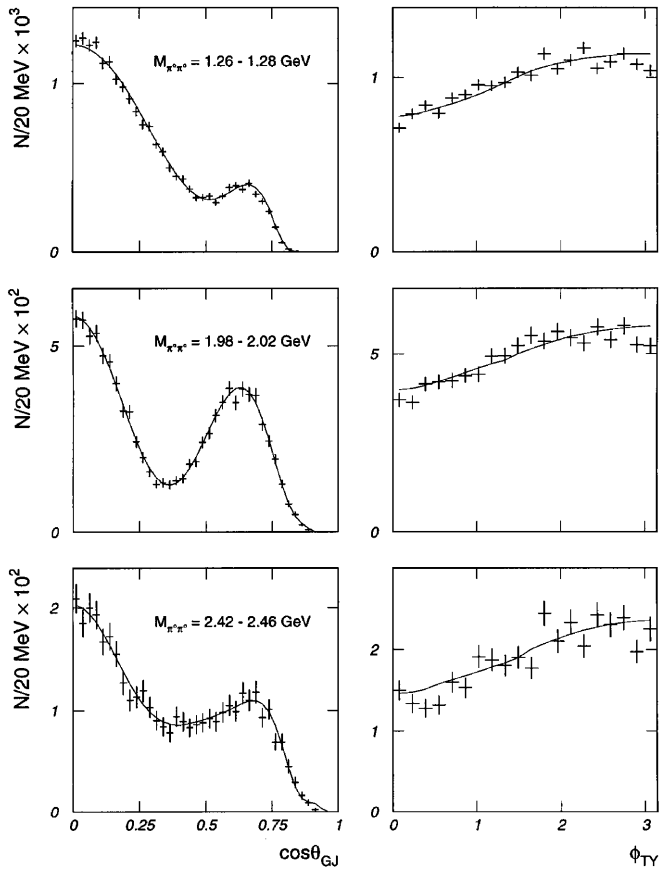

Fig. 6. Angular distributions of reaction (1) in the Gottfried-Jackson frame at the maxima of the $f_2(1270)$ (two upper plots), $f_4(2050)$ (two middle plots) and $f_6(2510)$ peaks. Curves show the theoretical distributions multiplied by the detection efficiency

of the amplitudes with natural and unnatural spin-parity exchange ($|m| = 1$) in the resonance region. This model works well for the D_- and D_+ waves at 38 GeV/c [1], amplitude modules of these waves are equal to each other not only in the $f_2(1270)$ mass region but at higher masses also. In our analysis two constraints, $|D_+| = |D_-|$ and $|G_+| = |G_-|$, predicted by the Ochs-Wagner model are applied. A quality of the angular distribution fit for one of the mass bins at the $f_2(1270)$ peak is shown in Fig. 6. In other bins the quality is similar.

Eight non-trivial PWA solutions are found by the method described above. One can reduce significantly the number of solutions by using some physical requirements. Of all solutions four are characterized by the unphysical behaviour of the G-waves at low masses (clear peaks in the $f_2(1270)$ region). Furthermore, some solutions do not comply with phase coherence for the D_0 and D_- waves in the $f_2(1270)$ mass region and for the G_0 and G_- waves in the $f_4(2050)$ mass region. All these solutions are excluded from further consideration. The only solution complying with the physical conditions is shown in Fig. 7. It should be noted that the behaviour of the relative phases of the D_0 and D_- waves as well as the G_0 and G_- waves agrees

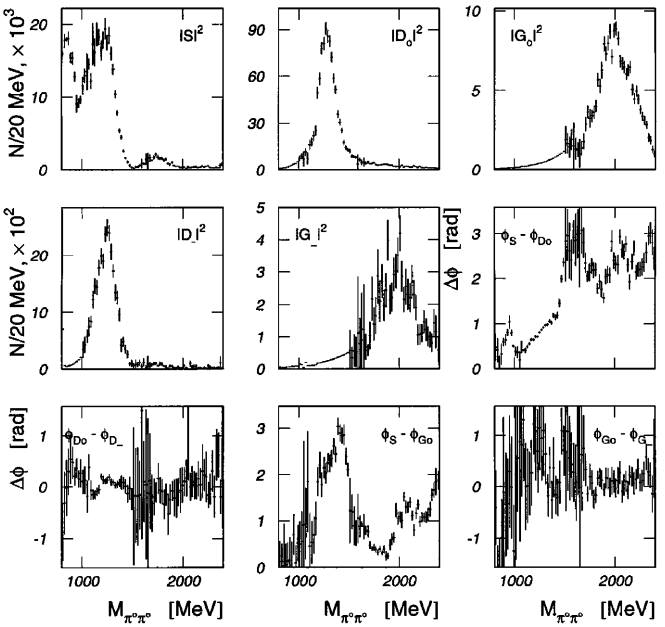

Fig. 7. Physical solution obtained in PWA with S, D and G waves

well with phase coherence. In a PWA with S, D, G and J waves phase coherence is applied to decrease the number of angular distribution parameters.

5.2 PWA in the mass region up to 3 GeV

To study a high mass region a PWA is carried out from 1.8 GeV to 3 GeV in 40 MeV mass bins with S, D_0, D_-, D_+, G_0, G_-, G_+, J_0, J_- and J_+ waves taken into account. Contribution of the J_- and J_+ waves is found to be equal to zero within the statistical errors. These waves are not taken into account in further analysis. In order to reduce the number of parameters to be determined from the angular distribution fit, a series of constraints is applied. First, it is required $|D_+| = |D_-|$ and $|G_+| = |G_-|$ in accordance with the Ochs-Wagner model. Then, phase coherence is applied: $\phi_{D_0} = \phi_{D_-}$ and $\phi_{G_0} = \phi_{G_-}$. At last, it is found that phase differences of the waves with natural and unnatural spin-parities ($|m| = 1$) corresponding to the same l are identical within the error bars. This allows one to put these phase differences to be equal to each other: $\phi_{G_+} - \phi_{D_+} = \phi_{G_-} - \phi_{D_-}$. In our PWA there are nine real parameters to be determined in each mass bin: six amplitude modules $|S|$, $|D_0|$, $|D_-|$, $|G_0|$, $|G_-|$, $|J_0|$, and three relative phases $\phi_{D_0} - \phi_S$, $\phi_{D_0} - \phi_{G_0}$ and $\phi_{D_0} - \phi_{J_0}$. All phases are measured relative to the D_0-wave phase because there are no resonance structures in this wave above the $f_2(1270)$ (see [5]), therefore the D_0-wave phase is nearly constant at high masses. A quality of the angular distribution fit for two mass bins in the maxima of the $f_4(2050)$ and $f_6(2510)$ peaks is shown in Fig. 6.

32 non-trivial PWA solutions found by the method described above may be classified into two equal sets. The

solutions from one of these sets are rejected because of the unphysical behaviour of the J-wave. A clear peak is seen in the J_0-wave at $f_4(2050)$ mass. Also a significant J_--wave with unphysical structure around 2 GeV appears in these solutions.

Each of the other 16 solutions exhibits a clear $f_6(2510)$ peak in the J_0-wave, below this peak the J_0-wave intensity decreases smoothly to zero. The J_--wave does not exhibit any statistically significant structure, its intensity is equal to zero within the error bars for each solution. The G_0-wave exhibits a clear $f_4(2050)$ peak for all 16 solutions while the G_--wave demonstrates various behaviours for different solutions. The $f_4(2050)$ is seen as a prominent peak in eight solutions. In other eight solutions the G_--wave intensity decreases monotonously with mass decrease, a shoulder is seen at 2 GeV. The G_0-wave for these solutions has a noticeable background but the $f_4(2050)$ signal is an order of magnitude higher in this wave as compared to the G_--wave, and $f_4(2050)$ is observed as a clear peak against a background of about 20%. Such a structure of the G-waves may be explained by their unphysical behaviour at low masses. The G-waves exhibit peaks in the $f_2(1270)$ region (see Sect. 5.1), the tails of these peaks are extended to the higher masses. These eight solutions are eliminated also as unphysical ones.

In each of the retained eight solutions, the $f_4(2050)$ is clearly seen both in the G_0 and G_- waves, while the S, D_0 and D_- waves have different behaviour. There are statistically significant structures in the D_0 and D_- waves in the mass range of $1.8-2.5$ GeV in all but one solutions. This is in contradiction with the results of the PWA with S, D and G waves obtained in this work (see also [4]). According to these analyses, the intensities of the D_0 and D_- waves decrease smoothly above the $f_2(1270)$ peak. The only solution complied with these results is shown in Fig. 8. Below 1.8 GeV the physical solution obtained in PWA with S, D and G waves is shown (see Sect. 5.1).

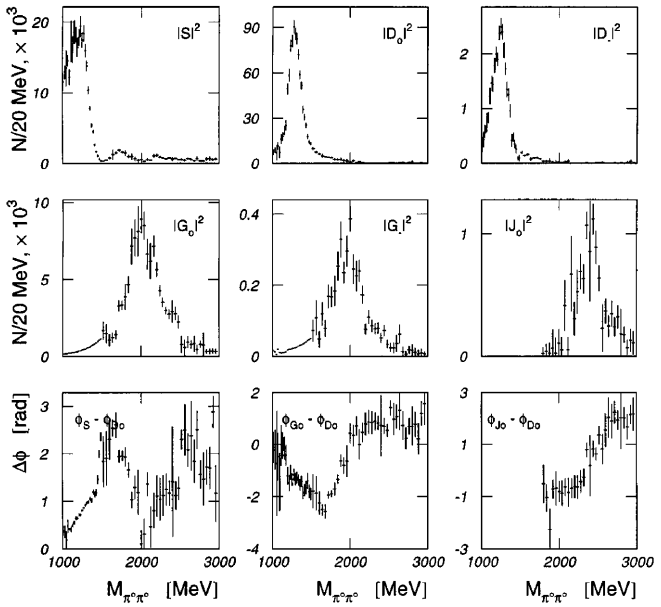

Fig. 8. Physical solution obtained in PWA with S, D, G and J waves

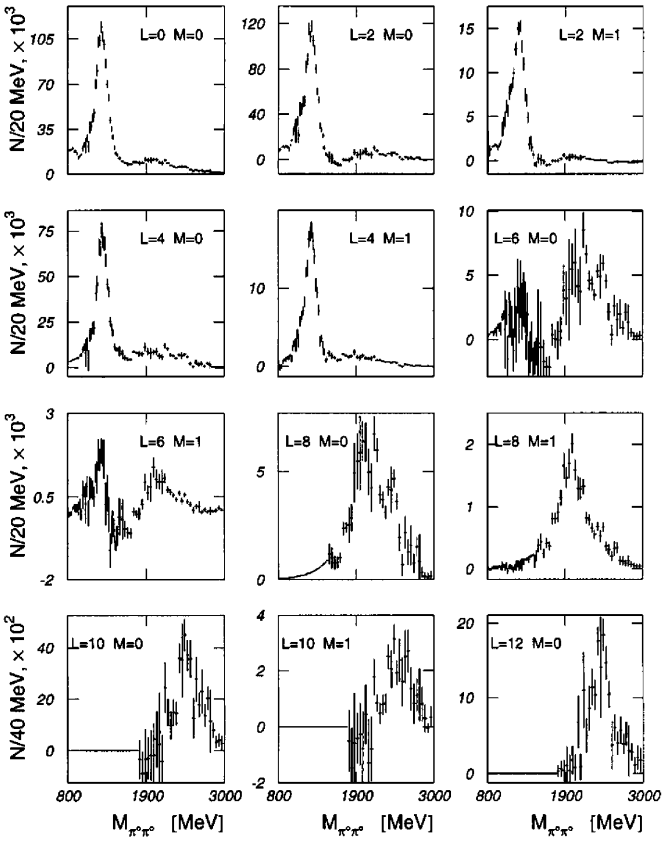

Fig. 9. Spherical harmonic moments restored from the partial amplitudes obtained in PWA with S, D, G and J waves

5.3 Spherical harmonic moments

Spherical harmonic moments $\sqrt{4\pi}t_L^M$ restored from the amplitudes are shown in Fig. 9 (the moments with $M \geq 2$ are equal to zero within the errors bars). The moments demonstrate features typical for all PWA solutions because they are determined unambiguously from the angular distributions. Clear $f_2(1270)$ peaks are seen in the moments with $L \leq 4$. Ratios of the t_M^0 and t_M^1 at mass of the $f_2(1270)$ allow one to estimate the ratio of the D_- and D_0 wave intensities (on condition that one can neglect the S and G wave contributions at this mass):

$$\begin{aligned} \frac{|D_-|^2}{|D_0|^2} &\approx \frac{1}{2}\left(\frac{t_2^1}{t_2^0}\right)^2 \approx 0.035, \\ \frac{|D_-|^2}{|D_0|^2} &\approx \frac{5}{3}\left(\frac{t_4^1}{t_4^0}\right)^2 \approx 0.037. \end{aligned} \qquad (12)$$

These estimations appear to be somewhat larger than the value obtained from the analysis in term of amplitudes, which can be explained by the approximate character of Eqs. (12).

The $f_4(2050)$ is clearly seen in the t_6^0 and t_6^1. A signal from this meson becomes more prominent in the moments

with $L = 8$ because these moments (t_8^0 and t_8^1) are expressed via G-amplitudes only (the J_0-wave gives negligibly small contribution at 2 GeV):

$$\sqrt{4\pi}t_8^0 = \frac{490\sqrt{17}}{2431}|G_0|^2 - \frac{392\sqrt{17}}{2431}\left(|G_-|^2 + |G_+|^2\right),$$
$$\sqrt{4\pi}t_8^1 = \frac{294\sqrt{85}}{2431}|G_0||G_-|\cos(\phi_{G_0} - \phi_{G_-}). \quad (13)$$

If one puts $\phi_{G_0} = \phi_{G_-}$ and $|G_+| = |G_-|$, the values of $|G_-|$ and $|G_0|$ can be easily determined from Eqs. (13). In the $f_4(2050)$ mass region a $|G_-|^2/|G_0|^2$ ratio is equal to 0.026 in a good agreement with the PWA results in terms of partial waves.

The t_{12}^0 is proportional to the $|J_0|^2$. A clear $f_6(2510)$ peak is seen in this moment.

5.4 Discussion

The behaviour of the physical solution found in this work is in good agreement with the results obtained at 38 GeV/c [1,4,5]. The S-wave has rather a complicated structure (Fig. 10). It demonstrates a series of four bumps separated with three dips, at 1, 1.5 and 2 GeV. The first two dips were observed earlier at 38 GeV/c. The former is associated with the $f_0(980)$, this scalar meson was studied in detail in [2,3,19]. The bump at 1.5 GeV seen previously in [4,5] is attributed to another scalar resonance, $f_0(1500)$, a ground state scalar glueball candidate. The S-wave structure above 2 GeV is less prominent at 38 GeV/c due to insufficient detection efficiency [5]. At 100 GeV/c the efficiency at high masses is much better, because of this a dip is clearly seen in the S-wave at 2 GeV followed by one more bump. It is important to note that the last bump appeared when the J_0-wave was added in PWA model (Sect. 5.2). The analysis with S, D and G waves only did not reveal any structure in the S-wave above 2 GeV (Fig. 7). A similar situation took place with the bump at 1.7 GeV [4]. It appeared in the S-wave after S, D and G waves have been taken into account correctly. In the first analysis [1], where apart from S, D_0, D_- and D_+ waves only G_0-wave was included with the $f_4(2050)$ tabulated parameters, the bump in the S-wave at 1.7 GeV was absent. It shows once more the importance of high wave account for correct determination of the S-wave at high masses.

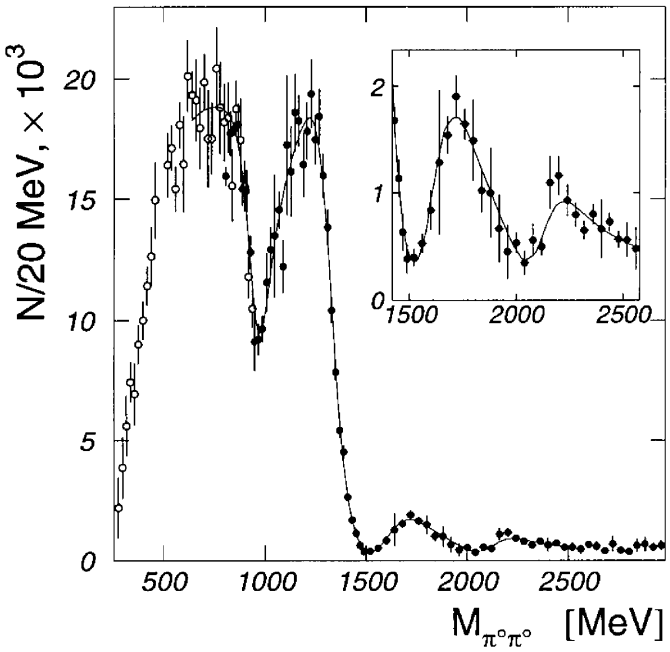

Fig. 10. S-wave amplitude module squared for the physical solution. Below 1 GeV the values of $|S|^2$ obtained at 38 GeV/c [18] are shown by open circles normalized to the present data. High mass region is shown in insertion. A curve shows the fit with the dependence described in the text

The S-wave phase measured relative to the D_0-wave phase has rather a complicated behaviour. It increases sharply around 1.5 GeV, confirming the presence of the $f_0(1500)$. The phase changes rapidly at 2 GeV as well. Along with the dip in the S-wave, this indicates the existence of a scalar resonance in this mass range. Such conclusion is confirmed by the results of $\eta\eta$-system study at 100 GeV/c [20]. The S-wave for one of two solutions found in [20] demonstrates above the $\eta\eta$-threshold a behaviour, similar to the behaviour of the S-wave, obtained in the present work. It shows three bumps, separated by dips at 1.45 GeV and 1.9 GeV.

The behaviour of the D and G waves is in good agreement with the Ochs-Wagner model prediction. A ratio of D_0 and D_- wave intensities at $f_2(1270)$ mass is about 3%. The same ratio obeys for G_0 and G_- wave intensities at mass of the $f_4(2050)$.

The G_0-wave phase measured relative to the D_0-wave phase changes by π at 2 GeV confirming the presence of the $f_4(2050)$. The relative phase of the J_0 and D_0 waves demonstrates a similar behaviour in the $f_6(2510)$ mass region.

6 Resonance parameters and production cross sections

6.1 Scalar resonances

To estimate the parameters and production cross sections of the scalar resonances produced in reaction (1), a fit to the S-wave amplitude module squared is carried out. The following parametrization is used

$$A(M_{\pi\pi}) = G(M_{\pi\pi}) + \sum_{n=1}^{N_{\rm res}} a_n e^{i\theta_n} B_n(M_{\pi\pi}), \quad (14)$$

$$G(M_{\pi\pi}) = (M_{\pi\pi} - 2m_{\pi^0})^\alpha e^{-\beta M_{\pi\pi} - \gamma {M_{\pi\pi}}^2}, \quad (15)$$

where a_n and θ_n are the amplitude and phase of the n-th resonance, respectively, α, β and γ are real parameters. A relativistic formula [21] is used for the Breit-Wigner

function $B(M_{\pi\pi})$:

$$B(M_{\pi\pi}) = \left(\frac{M_{\pi\pi}}{\sqrt{q}}\right)\sqrt{2l+1}\frac{M_R\Gamma}{M_R^2 - M_{\pi\pi}^2 - iM_R\Gamma}, \quad (16)$$

$$\Gamma = \Gamma_R\left(\frac{q}{q_R}\right)^{2l+1}\frac{D_l(q_R r)}{D_l(qr)}, \quad (17)$$

where q is a π^0's momentum in c.m.s. of dipion, l, M_R and Γ_R are spin, mass and width of the resonance, respectively, q_R is a π^0's momentum at $M_{\pi\pi} = M_R$, r is interaction radius being equal to 1 Fm (fit results depend only slightly on this parameter), $D_l(x)$ is the Blatt-Weiscopf barrier factor [22].

Function (14) is convoluted with a Gaussian distribution

$$\zeta(M, M_{\pi\pi}) = C\exp\left\{\frac{(M - M_{\pi\pi})^2}{2\sigma(M)}\right\}, \quad (18)$$

$\sigma(M) = 0.009 + 0.021M$ GeV, in order to account for the experimental mass resolution:

$$|S(M_{\pi\pi})|^2 = \int dM\,\zeta(M, M_{\pi\pi})\,|A(M)|^2\,. \quad (19)$$

Apart from three resonances discussed in Sect. 5.4, one more scalar resonance around 1.3 GeV is needed to describe the S-wave amplitude module squared in the whole mass range under study. The fit quality deteriorates significantly without the $f_0(1300)$ especially for the bump at 1.3 GeV. The dip at 1.5 GeV appears due to destructive interference of the $f_0(1300)$ and $f_0(1500)$ with a non-resonant part of the S-wave (Fig. 10). As a result of the interference the $f_0(1500)$ mass is shifted to higher values as compared to the dip position.

To check the stability of the obtained results, we varied the low and the high edges of the mass interval. We tried also to use the Breit-Wigner function or polynomial instead of $G(M)$ in (14). Variations of the $f_0(980)$ and $f_0(1300)$ parameters lie within the statistical errors: $M = 960 \pm 10$ MeV and $\Gamma = 70 \pm 20$ MeV for the $f_0(980)$ and $M = 1315 \pm 30$ MeV and $\Gamma = 190 \pm 50$ MeV for the $f_0(1300)$. Mass and width of the $f_0(1500)$ are determined with larger errors: $M = 1580 \pm 80$ MeV, $\Gamma = 280 \pm 100$ MeV. As for the resonance corresponding to the dip at 2 GeV, for its mass and width, the following values are obtained

$$\begin{aligned} M &= 2010 \pm 60 \text{ MeV}, \\ \Gamma &= 240 \pm 100 \text{ MeV}. \end{aligned} \quad (20)$$

The errors shown in (20) include both systematical and statistical errors. In what follows this resonance will be called $f_0(2010)$. A scalar state with the same mass 2020 ± 35 MeV and slightly larger width 410 ± 50 MeV was observed in the $\pi^+\pi^-\pi^+\pi^-$ system produced in pp central collisions at 450 GeV/c [23].

The production cross sections of the scalar resonances are estimated using the number of events under the Breit-Wigner curves and normalized to the $f_2(1270)$ cross section (see below):

$$\sigma(\pi^- p \to f_0(980)n) \times \mathrm{BR}(f_0(980) \to \pi^0\pi^0) = 5,4 \pm 1,2 \text{ nb}, \quad (21)$$

$$\sigma(\pi^- p \to f_0(1300)n) \times \mathrm{BR}(f_0(1300) \to \pi^0\pi^0) = 70 \pm 15 \text{ nb}, \quad (22)$$

$$\sigma(\pi^- p \to f_0(1500)n) \times \mathrm{BR}(f_0(1500) \to \pi^0\pi^0) = 12 \pm 3 \text{ nb}, \quad (23)$$

$$\sigma(\pi^- p \to f_0(2010)n) \times \mathrm{BR}(f_0(2010) \to \pi^0\pi^0) = 3 \pm 1 \text{ nb}. \quad (24)$$

Data on the S-wave in the $\pi^0\pi^0$-system produced at 100 GeV/c obtained in the present work does not contradict to the existence of a fifth resonance [6]. This state can be identified with a wide bump in the S-wave extending from the threshold up to ~ 2.5 GeV with the dips against its background (Fig. 10). Use of the Breit-Wigner function instead of $G(M)$ (see (14)) to describe a non-resonant part of the S-wave gives an equally good fit (χ^2 divided by the number of freedom increase only slightly, from 0.98 to 1.07). According to [6] the broad resonance is crucial for large interference effects seen in the S-wave.

6.2 Resonances with higher spins

In order to determine the masses, widths and production cross sections of the resonances observed in the D, G and J waves, amplitude modules squared of these waves are fitted with the sums of the Breit-Wigner curves (16) and backgrounds.

The D_0-amplitude module squared is well described by the relativistic spin 2 Breit-Wigner resonance with a mass of 1283 ± 5 MeV and a width of 171 ± 10 MeV, which are in good agreement with the $f_2(1270)$ tabulated parameters [24] (Fig. 11). A peak in the D_--wave is not fitted with the Breit-Wigner function, which may be explained by distortions due to insufficient efficiency at low masses.

The $f_4(2050)$ parameters are found on the basis of the simultaneous fit to the D_0, G_0, G_- amplitude modules squared and the relative phase of the D_0 and G_0 waves (Fig. 11). Coherent sums of resonances (16) for spin 4 and backgrounds (complex constants) are used to describe the G_0 and G_- amplitudes. The D_0-amplitude is parametrized in a similar way, the $f_2(1270)$ parameters being fixed to their tabulated values. The fit gives the following values for the $f_4(2050)$ mass and width (taking into account a mass resolution, $\sigma_M = 50$ MeV at $M_{\pi\pi} = 2$ GeV):

$$\begin{aligned} M &= 1998 \pm 15 \text{ MeV}, \\ \Gamma &= 395 \pm 40 \text{ MeV}. \end{aligned} \quad (25)$$

The $f_6(2510)$ parameters are determined from a simultaneous fit to the D_0 and J_0 amplitude modules squared and the relative phase of these waves (Fig. 11). The J_0-amplitude is parametrized as a coherent sum of resonance (16) for spin 6 and a background (complex constant). The D_0-amplitude is described with a complex

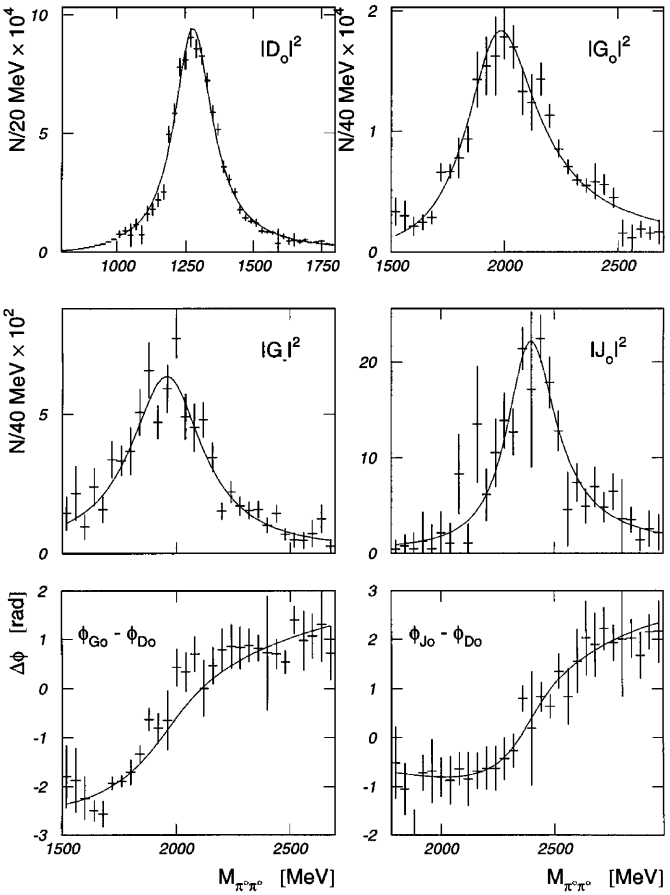

Fig. 11. Simultaneous fit to the G_0, G_- and J_0 amplitudes and relative phases of the G_0 and D_0, J_0 and D_0 waves (see details in the text)

polynomial of first order (D_0-amplitude parametrization in a form of the tail of the Breit-Wigner function gives unsatisfactory description). The following values are obtained for the $f_6(2510)$ mass and width:

$$M = 2420 \pm 30 \text{ MeV},$$
$$\Gamma = 270 \pm 60 \text{ MeV}. \quad (26)$$

The width is determined taking into account a mass resolution ($\sigma_M = 60$ MeV at $M_{\pi\pi} = 2.4$ GeV).

Production cross sections of the $f_4(2050)$ and $f_6(2510)$ are normalized to the cross section of the $f_2(1270)$ measured in one of our previous works with an accuracy of 8% [1]. The production cross section of the $f_2(1270)$ is equal to 326 ± 30 nb at 100 GeV/c. This value is obtained using the following energy dependence of the cross section [25]

$$\sigma(\pi^- p \to f_2(1270)n) \times \mathrm{BR}(f_2(1270) \to \pi^0\pi^0) = (2.61 \pm 0.20)\ \mu\mathrm{b}\ (p_{\mathrm{lab}}/38\ \mathrm{GeV/c})^{-2.15\pm0.05}. \quad (27)$$

A total number of the $f_2(1270)$ mesons detected in the D_0, D_- and D_+ waves is equal to $(1.25\pm0.02)\times10^6$, a corresponding sensitivity of the experiment is 0.261 ± 0.024 pb per one event of reaction (1). A ratio of the production cross sections of the $f_2(1270)$ in the D_- and D_0 waves is found to be 0.026 ± 0.002, being two times smaller as compared to the value of 0.059 ± 0.006 obtained at 38 GeV/c [1].

The production cross sections of the $f_4(2050)$ in the G_0 and $G_\pm$ waves at 100 GeV/c are found to be

$$\sigma_{G_0}(\pi^- p \to f_4(2050)n) \times \mathrm{BR}(f_4(2050) \to \pi^0\pi^0) = 74.8 \pm 7.2 \text{ nb}, \quad (28)$$

$$\sigma_{G_\pm}(\pi^- p \to f_4(2050)n) \times \mathrm{BR}(f_4(2050) \to \pi^0\pi^0) = 2.5 \pm 0.3 \text{ nb}. \quad (29)$$

A total $f_4(2050)$ production cross section in three G-waves (on condition that $|G_+| = |G_-|$) is equal to

$$\sigma_{\mathrm{tot}}(\pi^- p \to f_4(2050)n) \times \mathrm{BR}(f_4(2050) \to \pi^0\pi^0) = \sigma_{G_0} + 2\sigma_{G_-} = 79.8 \pm 7.8 \text{ nb}. \quad (30)$$

A ratio of the $f_4(2050)$ production cross sections in the G_- and G_0 waves is 0.033 ± 0.003. A similar ratio measured at 38 GeV/c is more than two times larger, 0.075 ± 0.007 [4].

The $f_6(2510)$ production cross section in the J_0-wave at 100 GeV/c is found to be

$$\sigma_{J_0}(\pi^- p \to f_6(2510)n) \times \mathrm{BR}(f_6(2510) \to \pi^0\pi^0) = 9.9 \pm 1.4 \text{ nb}. \quad (31)$$

An upper limit is set for the $f_6(2510)$ production cross section in the $J_\pm$-waves at 95% confidence level

$$\frac{\sigma_{J_\pm}(\pi^- p \to f_6 n) \times \mathrm{BR}(f_6 \to \pi^0\pi^0)}{\sigma_{J_0}(\pi^- p \to f_6 n) \times \mathrm{BR}(f_6 \to \pi^0\pi^0)} < \frac{1}{10}. \quad (32)$$

It is interesting to compare the results obtained in this work with the Ochs-Wagner model predictions. According to the model

$$\frac{|A^l_-|^2}{|A^l_o|^2} = \frac{c_A}{M^2_{\pi\pi}} l(l+1), \quad (33)$$

where A^l_0 and A^l_- are the amplitudes with unnatural-parity exchange corresponding to $|m| = 0$ and 1, respectively.

By using Eq. (33), one can calculate a $|G_-|^2/|G_0|^2$ ratio at mass of the $f_4(2050)$ from the D_- and D_0 wave intensities in the $f_2(1270)$ mass region. This ratio is equal to 0.034. A similar ratio for the J_- and J_0 waves in the $f_6(2510)$ mass region is equal to 0.051. Both values are in good agreement with the results obtained in the present work.

Ratios of the production cross sections of the $f_2(1270)$ in the D_0 and $D_\pm$ waves and of the $f_4(2050)$ in the G_0 and $G_\pm$ waves at 38 GeV/c and 100 GeV/c are found to be

$f_2(1270)$ meson, D_0-wave :
$$\sigma_{(100\ \mathrm{GeV/c})}/\sigma_{(38\ \mathrm{GeV/c})} = 0.134 \pm 0.016; \quad (34)$$

$f_2(1270)$ meson, $D_\pm$-waves :
$$\sigma_{(100\ \mathrm{GeV/c})}/\sigma_{(38\ \mathrm{GeV/c})} = 0.054 \pm 0.007; \quad (35)$$

$f_4(2050)$ meson, G_0-wave :
$$\sigma_{(100\ \mathrm{GeV/c})}/\sigma_{(38\ \mathrm{GeV/c})} = 0.106 \pm 0.016; \quad (36)$$

$f_4(2050)$ meson, $G_\pm$-waves :
$$\sigma_{(100\ \mathrm{GeV/c})}/\sigma_{(38\ \mathrm{GeV/c})} = 0.046 \pm 0.007. \quad (37)$$

It is seen from (34)–(37) that energy dependence of the production cross sections is essentially the same both for the $f_2(1270)$ and $f_4(2050)$.

7 Conclusion

A partial wave analysis of the $\pi^0\pi^0$-system produced in the $\pi^- p \to \pi^0\pi^0 n$ reaction at 100 GeV/c has been carried out taking into account S, D, G and J waves. The unique physical solution is found in the whole mass range under study from 0.8 GeV to 3 GeV, its behaviour agrees well with the behaviour of the solutions obtained earlier at 38 GeV/c. The S-wave for the physical solution has rather a complicated structure with three dips at 1, 1.5 and 2 GeV. These dips appear due to destructive interference of the $f_0(980)$, $f_0(1300)$, $f_0(1500)$ and $f_0(2010)$ with the wide bump extending from the threshold up to ~ 2.5 GeV. Parameters and production cross sections of these resonances have been measured.

Mesons with high spins, $f_2(1270)$, $f_4(2050)$ and $f_6(2510)$, are produced in the $\pi^- p \to \pi^0\pi^0 n$ reaction via dominating one pion exchange with a small absorption (about 3% for the $f_2(1270)$ and $f_4(2050)$ and less when 10% for the $f_6(2510)$), which is in agreement with the Ochs-Wagner model prediction. Parameters and production cross sections of the $f_2(1270)$, $f_4(2050)$ and $f_6(2510)$ have been determined.

This work was supported, in part, by the Russian Foundation for Basic Research (grant 96-15-96633).

References

1. Prokoshkin, Yu.D., Kondashov, A.A.: Physics-Doclady **336**, 613 (1994); *Proc. Fifth Intern. Conf. on Hadron Spectroscopy HADRON'93*, Como, Italy, 1993, in Nuovo Cimento A **107**, 1903 (1994)
2. Prokoshkin, Yu.D., Kondashov, A.A., Sadovsky, S.A.: Physics-Doclady **342**, 473 (1995); *Proc. XXVII Intern. Conf. on High Energy Physics*, Glasgow, UK, 1994, p. 1407
3. Alde, D., et al.: Z. Physik C **66**, 375 (1995); CERN preprint PPE/94-157, Geneva, 1994
4. Kondashov, A.A., Prokoshkin, Yu.D., Sadovsky, S.A.: IHEP preprint 95-137, Protvino, 1995; *Proc. NAN'95 Intern. Conf., Moscow*, Russia, 1995, in Phys. Atom. Nucl. **59**, 1680 (1996)
5. Prokoshkin, Yu.D., Kondashov, A.A., Sadovsky, S.A.: Physics-Doclady **353**, 323 (1997); *Proc. XXVIII Intern. Conf. on High Energy Physics*, Warsaw, Poland, 1996, p. 474
6. Anisovich, V.V., Prokoshkin, Yu.D., Sarantsev, A.V.: Phys. Lett. B **389**, 388 (1997)
7. Binon, F.G., et al.: Lett. Nuovo Cimento **39**, 41 (1984); Phys. Atom. Nucl. **38** 1199 (1983)
8. Alde, D., et al.: Phys. Atom. Nucl. **44**, 120 (1985)
9. Alde, D., et al.: Nucl. Instr. Meth. A **240**, 343 (1985)
10. Kulik, A.V., et al.: IHEP preprint 85-17, Serpukhov, 1985
11. Sadovsky, S.A., Kondashov, A.A., Samoylenko, V.D.: *Proc. XXVI Intern. Conf. on High Energy Physics*, Dallas, USA, 1992, p. 1791
12. James, F., Ross, M.: MINUIT (long writeup), CERN Program Library, D506, Geneva, 1987
13. Costa, G., et al.: Nucl. Phys. B **175**, 402 (1980)
14. Sadovsky, S.A.: IHEP preprint 91-75, Protvino, 1991
15. Chung, S.U.: BNL preprint QGS-95-41, 1995
16. Chung, S.U.: BNL preprint QGS-96-32, 1996
17. Ochs, W., Wagner, F.: Phys. Lett. B **44**, 271 (1973)
18. Sadovsky, S.A.: *Proc. Third Intern. Workshop on Light Quark Meson Spectroscopy*, Tsukuba, 1992 (KEK report 92-8) p. 87
19. Anisovich, V.V., et al.: Phys. Lett. B **355**, 363 (1995)
20. Alde, D., et al.: Nucl. Phys. B **269**, 485 (1986)
21. Svec, M.: Phys. Rev. D **53**, 2343 (1996)
22. Blatt, J., Weiskopf, W.: *Theoretical nuclear physics*, Wiley, 1952, p. 359
23. Barberis, D., et al.: Phys. Lett. B **413**, 217 (1997)
24. Particle Data Group: Phys. Rev. D **52** 1 (1996)
25. Achasov, N.N., Shestakov, G.N.: Preprint TF-N19(189), Novosibirsk, 1991